2014 5th IEEE RAS & EMBS International Conference on
Biomedical Robotics and Biomechatronics (BioRob)
August 12-15, 2014. São Paulo, Brazil

A Preliminary Evaluation of a Flexible Needle Steering Algorithm Using Magnetic Resonance Images as Feedback

Pedro Moreira, Gert van de Steeg, Ferdi van der Heijden, Jurgen J. Fütterer and Sarthak Misra

***Abstract*— Needle-based procedures are commonly performed for cancer diagnosis and treatment. Imaging modalities are used to visualize the needle tip and the target during these needle insertion procedures. Among the available imaging techniques, magnetic resonance (MR) offers the best tissue contrast, where detection of an early stage cancer is possible. MR-guided needle insertions are currently performed with rigid needles, which have limited steerability. Flexible needles have been introduced to increase the steerability during the insertion. In this paper, we present a preliminary evaluation of a steering method for flexible bevel-tipped needles using MR as an imaging modality. The steering algorithm uses a needle deflection model to predict the tip motion and calculate the optimal rotation to reach the target. The best sequence of rotations are defined by an optimization algorithm based on the Nelder-Mead technique. The needle tip and the target are manually tracked through a graphical user interface. The needle is inserted by a device fabricated with MR-compatible material. The MR-guided flexible needle steering is evaluated by a series of insertions in two phantoms with real obstacles and targets. The average targeting error with flexible needles is 4.3mm, which is 28% lower than the values reported in the literature with rigid needles. The results indicate the feasibility of MR-guided flexible needle insertions.**

I. Introduction

Early detection and treatment are of major importance to reduce cancer mortality rate. Several diagnostic and treatment techniques require needle insertion procedures, such as biopsy and brachytherapy. The success of such techniques are closely dependent on the needle placement accuracy. During needle insertion procedures, medical imaging modalities are used by clinicians to identify the needle tip and the target locations. Ultrasound (US) imaging is the commonly used technique to guide the needle towards a target due to its simplicity and real-time imaging [1]. However, US images present a poor tissue contrast and an early stage cancer lesion might not be visible [2]. Computed tomography (CT) offers a better tissue contrast than US, but the lack of real-time imaging and the toxic radiation delivered to the patient are important shortcomings [3]. On the other hand, magnetic resonance (MR) imaging offers high resolution images of tissues, in which the detection of early stage cancers is possible, without toxic radiations. Nonetheless, MR-guided needle insertion faces many challenges due to the space constraints of the MR bore, concerns about MR compatibility and the difficulty of acquiring real-time images.

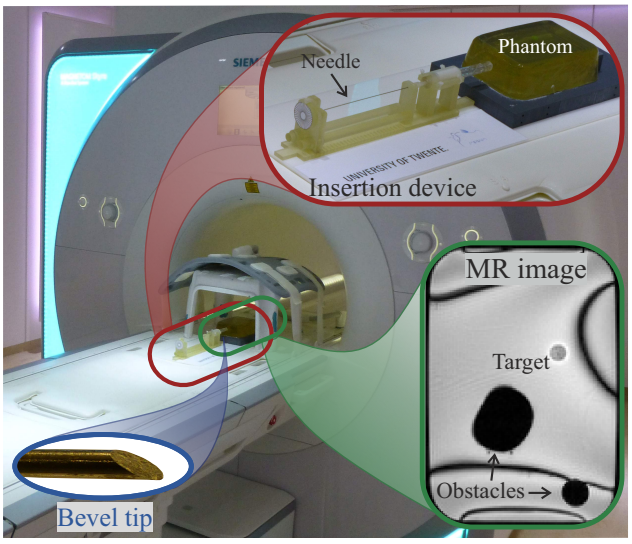

Fig. 1. A bevel-tipped flexible needle is steered towards a real target. The user inserts and axially rotates the needle into a phantom with obstacles using an insertion device. A magnetic resonance scanner is used as imaging modality to track the needle and the target.

Several robotic devices have been developed to assist MR-guided needle insertions. Fully automated MR-safe robotic systems have been developed to insert rigid and flexible needles [4], [5]. These systems are built with MR-compatible materials and the needle is driven by pneumatic or piezoelectric actuators. Semi-automated systems have been designed to robotically position the needle guide, allowing a manual needle insertion in the direction of the target [6], [7], [8]. Manual insertions are performed using thick and rigid needles while assuming that they follow a straight path. Those needles have limited steerability and may induce target motion by tissue deformation. In the last decade, the use of thin and flexible needles have been extensively studied in order to reduce patient discomfort, tissue deformation and also increase needle steerability [9], [10], [11]. However, those needles have not yet been used on needle-based procedures guided by MR images.

Several models and algorithms have been proposed to steer bevel-tipped flexible needles. Webster *et al.* [9] and Misra *et al.* [12] presented a kinematic and mechanics-based models to steer a bevel-tipped flexible needle, respectively. Two-dimensional (2D) steering algorithms are

The authors are affiliated with MIRA - Institute for Biomedical Technology and Technical Medicine (Robotics and Mechatronics Group), University of Twente, The Netherlands. Jurgen J. Fütterer is also affiliated with the Department of Radiology, Radboud University Nijmegen Medical Centre, The Netherlands.

This research is supported by funds from the Dutch Ministry of Economic Affairs and the Province of Overijssel, within the Pieken in de Delta (PIDON) Initiative, Project: MIRIAM (Minimally Invasive Robotics In An MRI environment).

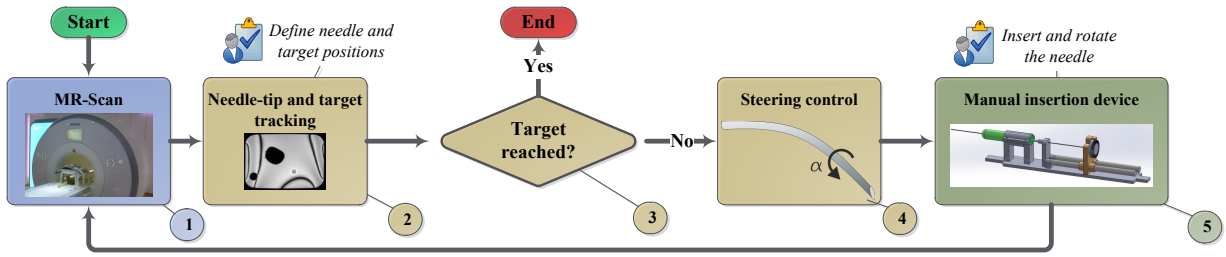

Fig. 2. At the start of the insertion a magnetic resonance (MR) scan is made (①). The clinician defines the needle tip and target positions on the MR image (②). If the target has not been reached (③), the steering algorithm calculates the rotation angle (α) that must be applied (④). The user rotates and inserts the needle using the manual insertion device (⑤). A new MR scan is performed and if the target has not been reached a new insertion step is performed.

presented by Minhas *et al.* [10] and Bernardes *et al.*[13] based on duty-cycled rotations. Recently, three-dimensional (3D) duty-cycling algorithms were presented by Moreira *et al.* [14] and Vrooijink *et al.* [15]. A steering algorithm based on the kinematic deflection model was presented by Abayazid *et al.* [11]. The extension to the 3D case was presented by Abayazid *et al.* [16]. All those steering methods need real-time imaging feedback to track the needle tip. The low image rate of MR and the lack of an MR-based needle tracking system make the needle steering with MR as imaging modality a challenging task. Although experiments have been performed to validate the MR-compatible robotic systems, MR-guided flexible needle steering experiments have not yet been demonstrated.

This work presents a needle steering algorithm specifically developed for MR-guided steering of a flexible bevel-tipped needle. The algorithm uses a needle deflection model to predict the needle tip motion and calculate the optimal needle axial rotation that minimizes the targeting error. To validate the proposed method, experiments steering a flexible bevel-tipped needle through a phantom are performed in an MR-Scanner (Fig. 1). To the best of our knowledge this is the first experimental study of MR-guided flexible needle steering.

The paper is organized as follows. In Section II, the methods for the MR-guided needle steering are described. Section III presents the experimental setup and results, followed by Section IV, which concludes and provides directions for future work.

II. Needle Steering Methods

In this section the methods used for the needle steering experiments are presented. The complete steering procedure is presented in Fig. 2. The clinician is expected to manually select the needle tip and the target positions on the MR image and insert the needle. The steering procedure is divided in steps. At each step the needle is rotated and a 15mm insertion is performed. This value is defined as the insertion step length (x_{ins}). The steering algorithm defines the needle rotation angle (α). The procedure is finished when the target is reached or the needle tip position exceeded the target position in the insertion direction. The needle deflection model and the steering algorithm are presented next, followed by the description of the graphical user interface.

A. Needle deflection model

The model predicts the needle tip position based on the needle rotation (α) and the insertion step length (x_{ins}). The predicted needle tip position $\left(\hat{\mathbf{p}}^0_{tip}(k+1)\right)$ in the reference frame ($\mathcal{S}_0$) is the sum of the current tip position $\left(\mathbf{p}^0_{tip}(k)\right)$ plus an incremental 3D tip motion (Fig. 3a). This incremental motion is a result of the needle insertion and deflection. Assuming that the needle tip follows a circular path [9], the 3D incremental tip motion for each step is defined as

$$r^2 = (x_t(k) - a)^2 + (y_t(k) - b)^2 + (z_t(k) - c)^2, \quad (1)$$

where (a, b, c) is the center of the circular motion, r is the radius, k is the step number, and $x_t(k)$, $y_t(k)$ and $z_t(k)$ are the components of the incremental tip motion. This incremental motion, in the tip coordinate frame ($\mathcal{S}_{tip}$), is a circular arc in the xz$_{tip}$-plane, as shown in Fig. 3b. Thus, the 3D needle tip path is composed of a sequence of 2D circular arcs performed at each insertion step. The center of the circular arc motion in the tip reference frame ($\mathcal{S}_{tip}$) is $(a, b, c) = (0, 0, -r)$. Using (1) we have

$$x_t^2(k) + z_t^2(k) + 2rz_t(k) = 0. \quad (2)$$

Assuming no axial compression of the needle, x_t is given by the following trigonometric relationship:

$$x_t(k) = r \sin\left(\frac{x_{ins}}{r}\right). \quad (3)$$

Using (2) and (3), the incremental needle tip motion $\left(\hat{\mathbf{p}}^{tip}_t(k)\right)$ in the needle tip frame ($\mathcal{S}_{tip}$) is written as

$$\hat{\mathbf{p}}^{tip}_t(k) = \begin{bmatrix} x_t(k) \\ y_t(k) \\ z_t(k) \end{bmatrix} = \begin{bmatrix} r\sin(\frac{x_{ins}}{r}) \\ 0 \\ \frac{2r - \sqrt{4r^2 - 4x_t^2(k)}}{2} \end{bmatrix} \quad (4)$$

The incremental tip motion is transformed from the tip frame ($\mathcal{S}_{tip}$) to the reference frame ($\mathcal{S}_0$) using a rotation matrix ($\mathbf{R}(k)$). At each insertion step the needle tip frame

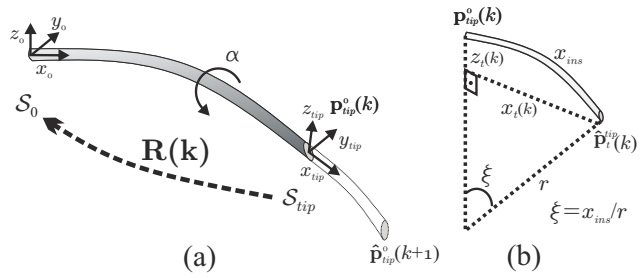

Fig. 3. (a) The needle deflection model predicts the needle tip position $\left(\mathbf{p}^0_t(k+1)\right)$ by calculating the incremental tip motion $\left(\mathbf{p}^{tip}_t(k)\right)$ and using the rotation matrix $(\mathbf{R}(k))$ from the needle tip frame $(\mathcal{S}_{tip})$ to the initial reference frame $(\mathcal{S}_0)$. The needle axial rotation $(\alpha(k))$ is an input for the needle deflection model. (b) The components of the incremental tip motion $(x_t(k),\, y_t(k),\, z_t(k))$ are calculated by a trigonometric relation between the insertion step length (x_{ins}), the radius of the circular motion (r) and the angle (ξ).

is rotated by the angle $(\theta(k))$ around the y-axis and by the rotation angle $(\alpha(k))$ around the x-axis (Fig. 3). These angles are used to calculate the rotation matrix $(\mathbf{R}(k))$. The angle $(\alpha(k))$ is an input to the needle deflection model and it is defined by the steering algorithm. The angle $(\theta(k))$ is the result of needle deflection and is approximated by

$$\theta(k) \approx \arctan\left(\frac{z_t(k-1)}{x_t(k-1)}\right). \tag{5}$$

The rotation matrix $\mathbf{R}(k)$ is given by

$$\mathbf{R}(k) = \mathbf{R}(k-1)\mathbf{R}_\alpha(k)\mathbf{R}_\theta(k) \tag{6}$$

where $\mathbf{R}_\alpha(k)$ is a rotation matrix around x-axis by the angle $(\alpha(k))$, $\mathbf{R}_\theta(k)$ is a rotation matrix around y-axis by the angle $(\theta(k))$. Thus, the needle tip position predicted by the deflection model is then written as

$$\hat{\mathbf{p}}^0_{tip}(k+1) = \mathbf{p}^0_{tip}(k) + \mathbf{R}(k)\hat{\mathbf{p}}^{tip}_t(k). \tag{7}$$

This needle deflection model is used in the steering algorithm to predict the needle tip motion.

B. Steering algorithm

The steering algorithm defines the needle rotation $(\alpha(k))$ for each insertion step. The rotations are used to orient the needle towards the target. Re-orientation of the needle is performed at each step. Therefore, it is important to optimize the sequence of rotations considering the next steps in order to minimize the targeting error.

A complete sequence of insertions and rotations to steer the needle from its current position to the target is calculated by the algorithm at each step (Fig. 4). The first value of the rotation sequence is applied and the needle is inserted by one insertion step length (x_{ins}). At the next step, the needle tip pose and the target position are updated with the values provided by the tip and target tracking. Then, a new sequence of rotation is calculated. An optimization function based on the Nelder-Mead method [17] is used to define the best rotation sequence that minimize the final targeting error $(\epsilon(k))$ given by

$$\epsilon(k) = \|\mathbf{p}_{tar}(k) - \hat{\mathbf{p}}_{tip-final}(k)\| \tag{8}$$

where $\mathbf{p}_{tar}(k)$ is the 3D target position and $\hat{\mathbf{p}}_{tip-final}(k)$ is the 3D final predicted needle tip position (Fig. 4). The targeting error is calculated at each iteration of the optimization function using the sequence of rotations and the needle deflection model presented in Section II-A. Typically, hundreds of iterations are necessary to define the optimal rotation sequence at each insertion step. The time necessary to run the steering algorithm at each step is usually less than 1 second, which is negligible if compared to the time necessary to perform the MR scan and track the needle tip (typically, 2 minutes).

C. Needle tip and target tracking

The needle tip and target positions are defined by the user through a graphical user interface implemented in Matlab (version R2013b, MathWorks, Natick, United States). After an MR scan is performed, an image data-set with the needle tip in-plane is created. The MR slices are manually aligned to the needle tip. The Digital Imaging and Communications in Medicine (DICOM) images are saved into a shared folder accessible from the graphical user interface. The images are displayed on the screen and the clinician indicates the target position, entry point, and needle tip pose (defined by two points) as illustrated in Fig. 5. The pose of the needle tip is calculated by the difference of the two selected tip points

$$\mathbf{m(k)} = \mathbf{n}_1(k) - \mathbf{n}_2(k), \tag{9}$$

where $\mathbf{n}_1$ and $\mathbf{n}_2$ are the two selected tip points and $\mathbf{m}$ is the needle tip orientation vector. The needle tip orientation is extracted from $\mathbf{m(k)}$ by using standard linear algebra techniques [18]. The coordinates of these points are then transformed into the frame $(\mathcal{S}_0)$, by means of the slice orientations which are incorporated in the DICOM files.

The needle position and orientation provided by the tracking are used by the steering algorithm to update the current needle pose. An algorithm for automated MR-based needle is beyond the scope of this work. Therefore, it is assumed that the manual input provided by the clinician is correct and accurate enough for the presented experiments.

III. Experiments

Experiments are conducted to validate the MR-guided needle steering method. The needle is steered towards a real target using a manual insertion device. The device components are made with polyjet 3D printing material, which makes the device MR-compatible (Fig. 6). A flexible nitinol needle with bevel tip angle of 30^o and diameter of 1mm is used in all experiments. The needle is rigidly attached to a dial with marks indicating the amount of axial needle rotation. Before each step, the user has to rotate the needle by the angle defined by the steering algorithm and insert the needle. A 15mm insertion step length (x_{ins}) is

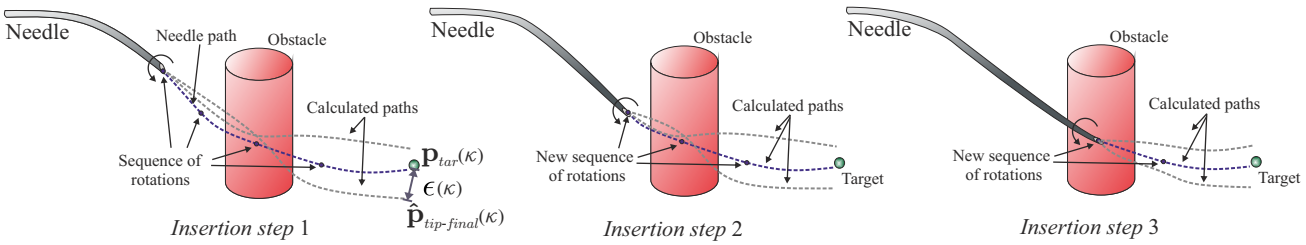

Fig. 4. The steering algorithm computes hundreds of paths to define the best sequence of rotations that minimize the final targeting error ($\epsilon(k)$) at each insertion step. The targeting error is defined by the distance between the predicted final needle tip position ($\hat{\mathbf{p}}_{tip-final}(k)$) and the target position ($\mathbf{p}_{tar}(k)$). The rotations are performed at each insertion step and the needle deflection model is used to predict the needle tip position at the subsequent steps.

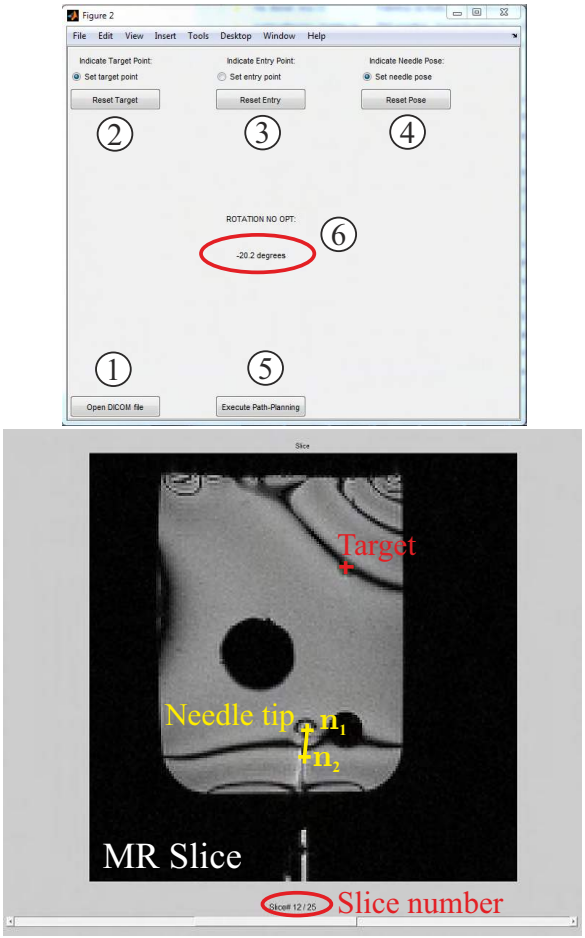

Fig. 5. The needle tip and the target are localized using a graphical user interface (GUI). The top figure shows the GUI window and bottom figure shows the MR slice loaded by the GUI. The GUI loads the DICOM files located in a shared folder, the clinician selects the needle and the target positions by clicking on the MR image. The needle tip position is defined by two points, $\mathbf{n}_1$ and $\mathbf{n}_2$. ① Open the DICOM data set. ② Select the target position. ③ Select the entry point. ④ Select the tip pose. ⑤ Run the steering algorithm. ⑥ Rotation angle to be applied.

defined for all experiments. The number of steps depends on the distance between the entry point and the target location, which can vary depending on the experiment.

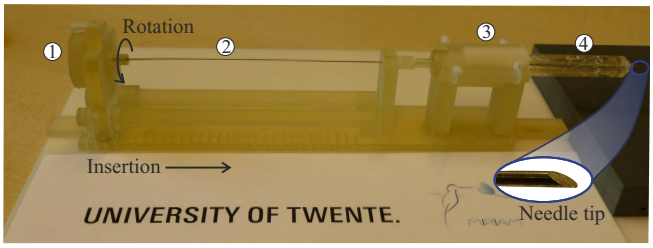

Fig. 6. The manual insertion and rotation device built with magnetic ressonance (MR) compatible material. The bevel-tipped flexible needle is attached to the device. ① Rotation dial. ② Flexible needle. ③ Needle guide holder. ④ Needle guide.

A. Experimental plan

Two phantoms are used to evaluate the steering algorithm, one without obstacles (Phantom 1) and one with two obstacles (Phantom 2), as shown in Fig. 7. The phantoms are prepared with a mixture of 80% water and 20% gelatin (Dr.Oetker, Ede, The Netherlands). This concentration provides a phantom with a Young's Modulus of $E \approx 90$kPa, which is within the range of prostate tissues' elasticity [19]. The Young's modulus is estimated using an US-based Acoustic Radiation Force Impulse imaging (ARFI) technique known as Virtual Touch^{TM} Quantification, available on the Siemens ACUSON S2000 US system (Siemens AG, Erlangen, Germany). The targets are made of a mixture of 80% water, 19.5% Polyvinyl alcohol (SigmaAldrich Chemie B.V., Zwijndrecht, The Netherlands) and 0.5% of green pigment. The targets are fabricated with a 4mm radius, which is within the range of the prostate tumors' size [20]. All experiments are performed in an MRI Scanner MAGNETOM Skyra (Siemens AG, Erlangen, Germany), using 25 T2 image slices, thickness of 4.0mm, field of view (FoV) of 256mm, echo time (TE) of 2.34ms and repetition time (TR) of 4.68mm. Four MR-guided needle steering experiments are performed. Two experiments are performed using Phantom 1 and two experiments are performed using Phantom 2.

B. Results

The needle insertion lengths of the experiments are between 70mm and 85mm. The target position with respect to the needle initial position ($\mathbf{p}^0_{tip}(0)$) and the sequence of

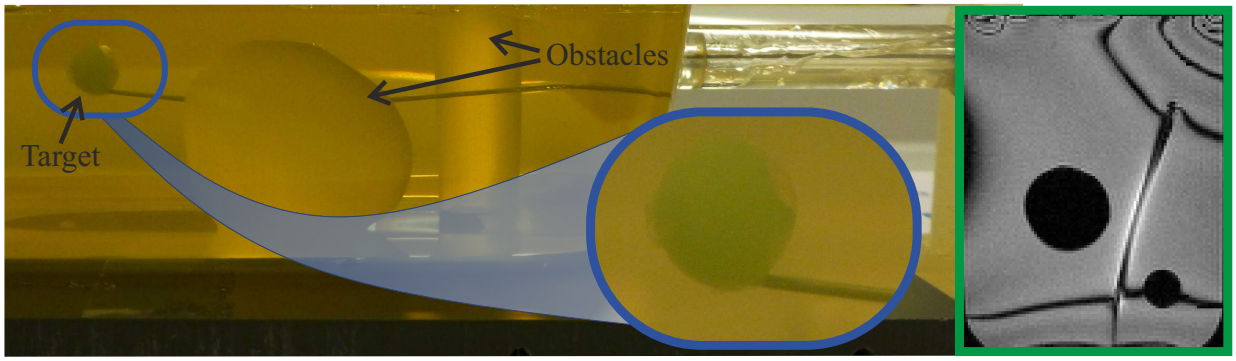

Fig. 8. Side view of a steering experiment in a phantom with obstacles (Experiment 3). The needle passes between the two obstacles and reaches the target with a targeting error of 5.3mm. On the right, the last magnetic resonance scan is presented, on which it is possible to see the two obstacles, the needle and the target.

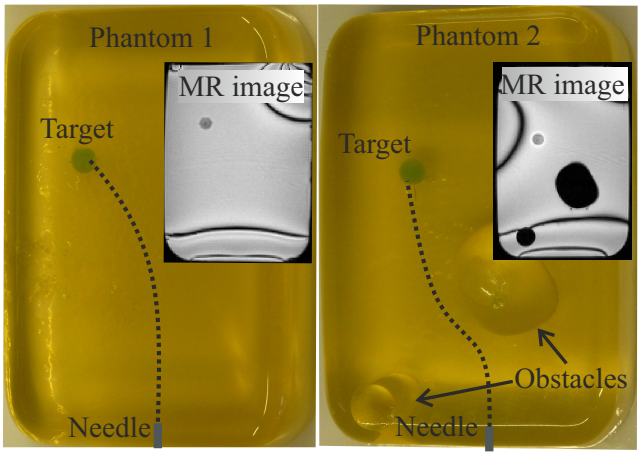

Fig. 7. Gelatin phantoms are used to validate the steering algorithm. The left figure shows the phantom without any obstacles and the right figure shows the phantom with obstacles. The magnetic resonance (MR) images of each phantom are also shown.

TABLE I

TARGET LOCATION WITH RESPECT TO THE NEEDLE INITIAL POSITION IN X-, Y- AND Z-AXIS, APPLIED ROTATIONS AT EACH STEP AND TARGETING ERROR FOR ALL FOUR PERFORMED EXPERIMENTS

	Phantom 1		Phantom 2	
Exp.	#1	#2	#3	#4
Target location	$x = 72$mm $y = 11$mm $z = 22$mm	$x = 71$mm $y = 18$mm $z = 12$mm	$x = 85$mm $y = -5$mm $z = 15$mm	$x = 81$mm $y = -9$mm $z = -6$mm
Step	Rotation (degrees)			
1	$+80°$	$+120°$	$-30°$	$-40°$
2	$-20°$	$+30°$	$+50°$	$-90°$
3	$-40°$	$-110°$	$-80°$	$+20°$
4	$+110°$	$+30°$	$-50°$	$0°$
5	$-10°$	$-40°$	$+20°$	$+60°$
6	–	–	$-30°$	$+40°$
Error	6.4mm	1.2mm	5.3mm	4.6mm

rotations defined by the steering algorithm are presented in Table I. The targeting errors for each experiment are also presented in Table I. The targeting error is defined by the distance between the final needle tip position and the center of the target. The rotations provided by the steering algorithm are rounded to multiples of $10°$ due to the resolution of the rotation dial. Each insertion step takes approximately 7 minutes. This is the total time taken to perform the MR scan, upload the images in the graphical user interface, select the needle tip and target locations, run the steering algorithm and perform the manual rotation and insertion.

The average targeting error of four experiments is 4.3mm. Fig. 8 shows the side view and the last MR scan of Experiment 3. One can observe that the needle passes between two obstacles and reaches the target as expected. The target is reached in Experiments 2, 3 and 4. In Experiment 1, the targeting error is 6.4mm, but the distance between the needle tip and the edge of the target is 2.4mm. In Experiments 3 and 4 the needle goes further and crosses the target, which results in an overshoot (i.e., distance between the final needle tip position and the edge of the target) of 1.3mm and 0.6mm, respectively. The overshoot can be reduced by using a smaller insertion step length. A few aspects of our experimental setup influence the targeting error and are discussed next.

C. Discussion

The results show the feasibility of steering a flexible needle using MR as an imaging modality. The accuracy achieved in our flexible needle steering experiments is better than the accuracy achieved by conventional rigid insertions. The results reported by Blumenfeld *et al.* [21] show that experienced clinicians perform MR-guided manual insertion of rigid needles with an accuracy between 5.5-6.5mm. However, several aspects of our experimental setup can be improved to reduce the targeting error. We could observe that aligning the MR slices to have the needle tip in plane is a difficult task and small misalignment leads to errors in the needle tip orientation. An automatic MR-based needle tracking system can improve the accuracy of the needle tip tracking. It is important to note that automatic needle tracking is an intricate, and still open, research problem. Inserting and rotating the needle manually are also important

sources of error. The use of robotic actuation to insert and rotate the needle may reduce the targeting error.

Automatic needle tip tracking and robotic needle actuation will also reduce the time to perform each insertion step. Nevertheless, the time spent in a complete needle insertion in this work is, on avarege, 19 minutes less than the time of a manual MR-guided prostate biopsy using a rigid needle. The average procedure time for an MR-guided prostate biopsy reported by Schouten et al. [7] is 61 minutes, while in our study is 42 minutes.

IV. Conclusions and future work

We presented an algorithm to steer a bevel-tipped flexible needle using MR as an imaging modality to detect the needle and target positions. MR-guided needle steering experiments are conducted in order to evaluate the algorithm and the feasibility of using flexible needle during MR-guided procedures. The needle is inserted and rotated by a manual insertion device fabricated with MR-compatible material. The needle and target position are manually tracked by the user through a graphical user interface. The steering algorithm uses the information provided by the needle tip tracking to calculate the best sequence of needle rotations that minimize the targeting error. The average targeting error achieved in our experiments is 4.3mm, and the average time to complete on insertion is 42min. These values are 28% (targeting error) and 31% (total time) lower than the values reported in the literature for MR-guided prostate biopsy using rigid needles. These preliminary results are promising and demonstrate the feasibility of MR-guided needle steering. However, additional experimental results are necessary in order to perform a complete statistical analysis of the targeting accuracy.

Future work will focus on improving the manual insertion device by increasing the accuracy of the rotation dial. An extensive study with several different phantoms and including biological tissues are planned to investigate the steering accuracy in inhomogeneous environments. We are currently developing an MR-based automatic needle tracking that should replace the need of manually selecting the needle and target locations on the MR image. Moreover, experiments using a MR-compatible robotic system are also planned and will improve the targeting accuracy and reduce the insertion time. Our current study demonstrates that it is possible to steer a flexible needle using MR images with better accuracy and in a shorter time than conventional MR-guided insertion of rigid needles. Additionally, it is important to highlight that the use of flexible needles enables clinicians to maneuver around anatomical obstacles and opens new possibilities of clinical MR-guided needle-based procedures.

References

[1] J. J. Fütterer, S. Misra, and K. J. Macura, "MRI of the prostate: potential role of robots," *Imaging in Medicine*, vol. 2, no. 5, pp. 583 – 592, 2010.

[2] P. C. Mozer, A. W. Partin, and D. Stoianovici, "Robotic image-guided needle interventions of the prostate," *Reviews in Urology*, vol. 1, no. 11, pp. 7–15, 2009.

[3] G. Fichtinger, T. L. DeWeese, A. Patriciu, A. Tanacs, D. Mazilu, J. H. Anderson, K. Masamune, R. H. Taylor, and D. Stoianovici, "System for robotically assisted prostate biopsy and therapy with intraoperative CT guidance," *Academic Radiology*, vol. 9, no. 1, pp. 60 – 74, 2002.

[4] R. Seifabadi, I. Iordachita, and G. Fichtinger, "Design of a teleoperated needle steering system for MRI-guided prostate interventions," in *IEEE RAS & EMBS International Conference on Biomedical Robotics and Biomechatronics (BioRob)*, Rome, Italy, June 2012, pp. 793–798.

[5] G. Li, H. Su, W. Shang, J. Tokuda, N. Hata, C. M. Tempany, and G. S. Fischer, "A fully actuated robotic assistant for MRI-guided prostate biopsy and brachytherapy," in *SPIE Medical Imaging Conference*, March 2013.

[6] D. Stoianovici, C. Kim, G. Srimathveeravalli, P. Sebrecht, D. Petrisor, J. Coleman, S. Solomon, and H. Hricak, "MRI-safe robot for endorectal prostate biopsy," *IEEE/ASME Transactions on Mechatronics*, vol. 19, no. 4, pp. 1289–1299, 2013.

[7] M. G. Schouten, J. G. R. Bomers, D. Yakar, H. Huisman, D. Bosboom, T. W. J. Scheenen, S. Misra, and J. J. Fütterer, "Evaluation of a robotic technique for transrectal MRI-guided prostate biopsies," *European Radiology*, vol. 22, no. 2, pp. 476–483, 2012.

[8] S. Abdelaziz, L. Esteveny, L. Barbé, P. Renaud, B. Bayle, and M. De Mathelin, "Development of a MR-compatible cable-driven manipulator: Design and technological issues," in *2012 IEEE International Conference on Robotics and Automation (ICRA)*, St. Paul, USA, 2012, pp. 1488–1494.

[9] R. J. Webster III, J. S. Kim, N. J. Cowan, G. S. Chirikjian, and A. M. Okamura, "Nonholonomic modeling of needle steering," *The International Journal of Robotics Research*, pp. 509 – 525, 2006.

[10] D. S. Minhas, J. A. Engh, M. M. Fenske, and C. N. Riviere, "Modeling of needle steering via duty-cycled spinning," in *Annual International Conference of the IEEE Engineering in Medicine and Biology Society (EMBC)*, Buenos Aires, Argentina, August 2007, pp. 5432 – 5435.

[11] M. Abayazid, R. J. Roesthuis, R. Reilink, and S. Misra, "Integrating deflection models and image feedback for real-time flexible needle steering," *IEEE Transactions on Robotics*, vol. 29, no. 2, pp. 542 – 553, 2013.

[12] S. Misra, K. B. Reed, B. W. Schafer, K. T. Ramesh, and A. M. Okamura, "Mechanics of flexible needles robotically steered through soft tissue," *International Journal of Robotics Research*, vol. 23, no. 13, pp. 1640–1660, 2010.

[13] M. Bernardes, B. Adorno, P. Poignet, and G. Borges, "Robot-assisted automatic insertion of steerable needles with closed-loop imaging feedback and intraoperative trajectory replanning," *Mechatronics*, vol. 23, no. 6, pp. 630 – 645, 2013.

[14] P. Moreira, S. Patil, R. Alterovitz, and S. Misra, "Needle steering in biological tissue using ultrasound-based online curvature estimation," in *2014 IEEE International Conference on Robotics and Automation (ICRA)*, Hong Kong, 2014, *Accepted*.

[15] G. J. Vrooijink, M. Abayazid, S. Patil, R. Alterovitz, and S. Misra, "Needle path planning and steering in a three-dimensional non-static environment using two-dimensional ultrasound images," *International Journal of Robotics Research*, 2014, *In Press* DOI: 10.1177/0278364914526627.

[16] M. Abayazid, G. J. Vrooijink, S. Patil, R. Alterovitz, and S. Misra, "Experimental evaluation of ultrasound-guided 3d needle steering in biological tissue," *International Journal of Computer Assisted Radiology and Surgery*, 2014, *In Press* DOI: 10.1007/s11548-014-0987-y.

[17] J. H. Mathews and K. K. Fink, *Numerical Methods Using Matlab*, 4th ed. Prentice-Hall, 2004.

[18] G. Vrooijink, M. Abayazid, and S. Misra, "Real-time three-dimensional flexible needle tracking using two-dimensional ultrasound," in *IEEE International Conference on Robotics and Automation (ICRA)*, May 2013, pp. 1688–1693.

[19] T. A. Krouskop, T. M. Wheeler, F. K. B. S. Garra, and T. Hall, "Elastic moduli of breast and prostate tissues under compression," *Ultrasonic Imaging*, vol. 20, no. 4, pp. 260 – 274, 1998.

[20] L. E. Eichelberger, M. O. Koch, J. K. Daggy, T. M. Ulbright, J. N. Eble, and L. Cheng, "Predicting tumor volume in radical prostatectomy specimens from patients with prostate cancer," *American Journal of Clinical Pathology*, vol. 120, no. 3, pp. 386 – 391, 2003.

[21] P. Blumenfeld, N. Hata, S. Dimaio, K. Zou, S. Haker, G. Fichtinger, and C. M. Tempany, "Transperineal prostate biopsy under magnetic resonance image guidance: A needle placement accuracy study," *Journal of Magnetic Resonance Imaging*, vol. 26, no. 3, pp. 688 – 694, 2007.